RSC Advances

PAPER

View Article Online
View Journal | View Issue

Cite this: *RSC Adv.*, 2025, **15**, 19872

Structural and luminescent properties of Dy^{3+}-doped Ca_3WO_6 phosphors for white-light display applications

P. N. K. Chaitanya, [a] D. Haranath, [*a] D. Dinakar, [a] M. Sree Ramana,[b] K. V. R. Murthy,[c] M. Rakshita [a] and Govind Gupta [d]

This study unveils the synthesis and in-depth characterization of Dy^{3+}-doped calcium tungstate (Ca_3WO_6) double perovskite phosphors, designed for advanced photoluminescence (PL) applications. These phosphors, with Dy^{3+} doping levels of 0.5–2.5 mol%, were synthesized using a high-temperature solid-state reaction method. Structural and morphological properties were rigorously evaluated through X-ray diffraction (XRD), scanning electron microscopy (SEM), and energy-dispersive X-ray spectroscopy (EDAX). Rietveld refinement of XRD data confirmed a monoclinic crystal structure, while SEM revealed a porous morphology attributed to high-temperature calcination, with EDAX verifying uniform elemental distribution. Excited at 278 nm, the Ca_3WO_6:Dy^{3+} phosphors emit intense white light, driven by the $^4F_{9/2} \rightarrow {}^6H_{15/2}$ (485 nm) and $^4F_{9/2} \rightarrow {}^6H_{13/2}$ (576 nm) transitions of Dy^{3+} ions. The effects of doping concentration on PL intensity and concentration quenching were thoroughly investigated. PL decay lifetime analysis at $\lambda_{ex} = 278$ nm and $\lambda_{em} = 576$ nm elucidated the decay kinetics, affirming the phosphor's high external quantum yield (~59%). CIE chromaticity coordinates place the emission squarely in the white light spectrum, underscoring the exceptional potential of these phosphors for advanced white light-emitting display technologies.

Received 15th April 2025
Accepted 6th June 2025

DOI: 10.1039/d5ra02648b

rsc.li/rsc-advances

1. Introduction

Trivalent lanthanide ions, distinguished by their unique 4f electronic configurations, are renowned for generating sharp, vibrant emission spectra arising from intra-4f electronic transitions. These characteristics render them indispensable in the realms of advanced optics, photonics, and materials science.[1,2] Among these ions, dysprosium (Dy^{3+}) stands out for its remarkable ability to produce white light through characteristic blue ($^4F_{9/2} \rightarrow {}^6H_{15/2}$, ~485 nm) and yellow ($^4F_{9/2} \rightarrow {}^6H_{13/2}$, ~576 nm) emissions, making it a pivotal dopant for cutting-edge applications in lighting, displays, and photonic devices.[3,4] The advent of phosphor-converted light-emitting diodes (pc-LEDs) has revolutionized the lighting industry, delivering unparalleled energy efficiency, exceptional brightness, and superior durability compared to conventional incandescent and fluorescent sources. Lanthanide-doped phosphors, including those activated by Dy^{3+}, europium (Eu^{3+}), terbium (Tb^{3+}), and other rare-earth ions, are integral to a wide array of applications, encompassing solid-state lighting, bioimaging, laser technologies, and high-resolution display systems.[5,6]

Double perovskite oxides, characterized by the general formula $A_2BB'O_6$, offer a highly versatile platform for luminescent materials due to their tunable structural, electronic, and optical properties.[7,8] The ordered cationic frameworks of these materials provide an ideal host lattice for lanthanide ion incorporation, significantly enhancing luminescent performance for applications in LEDs, plasma display panels, and non-volatile memory devices. Recent studies on Dy^{3+}-doped double perovskites, such as Ca_2MgWO_6:Dy^{3+} and Sr_2CaWO_6:-Dy^{3+}, have demonstrated exceptional luminescence properties, underscoring their potential for transformative photonic applications.[9–11] Among these hosts, calcium tungstate (Ca_3WO_6) emerges as a particularly promising candidate for Dy^{3+} doping, owing to its robust monoclinic crystal structure, high thermal stability, and low phonon energy. These attributes minimize non-radiative relaxation pathways, thereby enhancing luminescence efficiency. The tungstate (WO_6^{2-}) polyhedral units within Ca_3WO_6 create an optimal crystal field environment that facilitates efficient energy transfer to Dy^{3+} ions, amplifying their radiative emission. However, the substitution of divalent Ca^{2+} with trivalent Dy^{3+} introduces a charge imbalance, necessitating compensatory mechanisms such as cation vacancies, interstitial ions, or co-doping strategies. These

[a]*Department of Physics, National Institute of Technology, Warangal-506004, India. E-mail: haranath@nitw.ac.in ; praturi.chaitanya@gmail.com*

[b]*DLS, Vignayanakancha, RCI, Hyderabad-500069, India*

[c]*Applied Physics Department, Faculty of Technology and Engineering, The Maharaja Sayajirao University of Baroda, Vadodara-390001, India*

[d]*Sensor Devices & Metrology, CSIR-National Physical Laboratory, Dr. K.S. Krishnan Road, New Delhi 110 012, India*

mechanisms can profoundly influence defect formation, local site symmetry, and concentration quenching, all of which are critical factors in determining the luminescent performance of the phosphor. A comprehensive understanding of these phenomena is essential for tailoring Ca_3WO_6:Dy^{3+} phosphors to meet the stringent requirements of advanced LEDs, high-resolution displays, and scintillation detectors.

This study systematically investigates the luminescent properties of Dy^{3+}-doped Ca_3WO_6, with a focus on optimizing Dy^{3+} doping concentration and synthesis parameters to maximize emission efficiency and color tunability. The down-conversion luminescence behavior was rigorously characterized under excitation wavelengths of 278 nm, 353 nm, and 388 nm, employing photoluminescence (PL) spectroscopy, decay kinetics analysis, and CIE chromaticity coordinate evaluation. These analyses elucidate the phosphor's suitability for high-performance display technologies and white-light-emitting devices. The novelty of this work lies in achieving unprecedented luminescence efficiency and precise chromaticity control through tailored synthesis and doping strategies, paving the way for significant advancements in white LED technology and next-generation photonic systems. By leveraging the unique structural and optical properties of Ca_3WO_6:Dy^{3+}, this research establishes a robust foundation for the development of transformative optical materials, poised to redefine the landscape of solid-state lighting and advanced display technologies.

2. Materials synthesis and characterization

2.1. Synthesis of Ca_3WO_6:Dy^{3+} phosphors

A series of white-emitting Ca_3WO_6:Dy^{3+} double perovskite phosphors, doped with Dy^{3+} concentrations ranging from 0.5 to 2.5 mol%, was synthesized *via* a high-temperature solid-state reaction method. Six samples, including an undoped Ca_3WO_6 host, were prepared, each with a 5 gram batch size. High-purity precursors such as $CaCO_3$ (99%), WO_3 (99.9%), and Dy_2O_3 (99.9%) were weighed in precise stoichiometric ratios. The precursors were meticulously blended and ground for 30 minutes using an agate mortar and pestle, with acetone as a mixing medium to achieve uniform dispersion. The homogenized mixture was transferred to an alumina crucible and calcined at 1200 °C for 6 hours in a muffle furnace under an ambient air atmosphere. After calcination, the samples were slowly cooled to room temperature and finely pulverized to produce high-quality phosphor powders ready for characterization.

2.2. Characterization

To comprehensively investigate the structural, morphological, and luminescent properties of the as-synthesized Ca_3WO_6:Dy^{3+} phosphors, a multifaceted characterization approach was employed. Structural properties were analyzed using X-ray diffraction (XRD) on a Rigaku SmartLab SE diffractometer with Cu Kα radiation ($\lambda = 1.5406$ Å). Diffraction patterns were collected over a 2θ range of 10–70° at a scan rate of 5° min^{-1}, ensuring precise assessment of phase purity and crystallographic parameters. Morphological features were examined *via* a Carl Zeiss Supra 55 scanning electron microscope (SEM), with micrographs acquired at resolutions of 200 nm, 1 μm, and 2 μm to evaluate particle size, shape, and surface morphology. Elemental composition and distribution were confirmed using energy-dispersive X-ray spectroscopy (EDAX) integrated with the SEM system. Surface chemical states were probed through X-ray photoelectron spectroscopy (XPS) on an OMICRON Multiprobe Surface Analysis System, operating at a base pressure of 5×10^{-11} torr. Photoluminescence (PL) properties were characterized using a Shimadzu Spectrofluorophotometer equipped with a xenon lamp, capturing excitation and emission spectra at ambient temperature to elucidate the phosphors' optical performance. This rigorous, systematic characterization framework provides a robust foundation for understanding the phosphors' suitability for advanced photonic applications. The external quantum yield (QY) measurements on the samples have been carried out using Stellar Net Inc., USA made Integrating Sphere (IS6) attached to the PL instrument.

3. Result and discussion

3.1. XRD phase analysis

X-ray diffraction (XRD) analysis, a pivotal tool for decoding the crystalline architecture of materials, was employed to probe the structural properties of the Ca_3WO_6 host matrix and its Dy^{3+}-doped variants. Powder XRD patterns were collected using a Rigaku SmartLab SE diffractometer with Cu Kα radiation ($\lambda = 1.5406$ Å), scanning a 2θ range of 10–70° at a rate of 5° min^{-1}. Structural refinement was performed *via* the Rietveld method using the FullProf Suite software, ensuring precise determination of crystal phase, lattice parameters, and unit cell characteristics.

The Rietveld-refined XRD pattern of undoped Ca_3WO_6, presented in Fig. 1, exhibits excellent agreement between experimental and calculated profiles, validating the material's structural integrity. The analysis confirmed a monoclinic crystalline structure with the $P2_1/c$ space group.[12] Key crystallographic parameters—lattice constants (a, b, c), unit cell volume, reliability factors (R_p, R_{wp}), and goodness-of-fit (χ^2)—were meticulously derived and are summarized in Table 1, offering a comprehensive structural profile. The calculated unit cell volume further reinforces the stability of the monoclinic phase.

Fig. 2 displays the XRD patterns of undoped and Dy^{3+}-doped Ca_3WO_6 phosphors, with Dy^{3+} concentrations ranging from 0.5 to 2.5 mol%. The sharp diffraction peaks reflect the high crystallinity and ordered atomic structure of the materials. Notably, the XRD profiles of doped phosphors closely resemble that of the undoped host, confirming that Dy^{3+} incorporation preserves the monoclinic $P2_1/c$ structure. Subtle peak intensity variations, attributed to the electronic effects of Dy^{3+} ions, were observed. The average crystallite sizes, calculated for Dy^{3+} concentrations of 0, 0.5, 1.0, 1.5, 2.0, and 2.5 mol%, were 22.78 nm, 21.98 nm, 22.56 nm, 22.66 nm, 22.02 nm, and 22.68 nm, respectively.

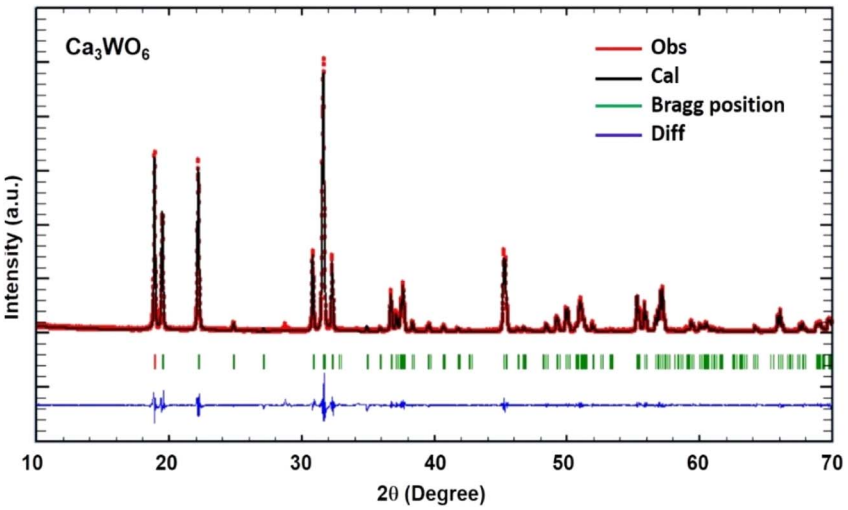

Fig. 1 Rietveld refined the X-ray diffraction profile of undoped Ca_3WO_6.

Table 1 Lattice parameters of pure Ca_3WO_6 double perovskite phosphor

Formula	Ca_3WO_6
Radiation	Cu Kα
2θ range	10–70°
Symmetry	Monoclinic
Space group	$P2_1/c$
a (Å)	5.54
b (Å)	5.79
c (Å)	7.98
β	90.20°
R_p	2.5
R_{wp}	3.5
χ^2	1.9
V (Å^3)	255.97

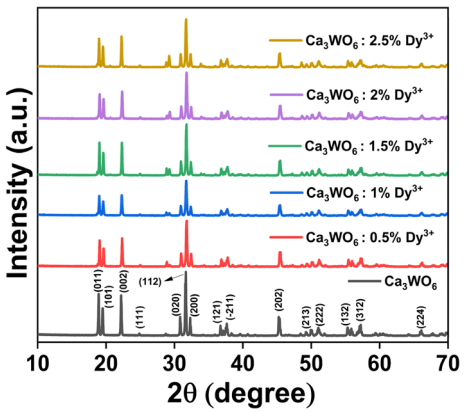

Fig. 2 Powder XRD patterns of Ca_3WO_6:x mol% Dy^{3+} (x = 0.5–2.5) phosphors.

To assess Dy^{3+} substitution compatibility, the percentage difference in ionic radii (D_r) between Dy^{3+} and host cations was calculated per Pires and Davolos.[13] With D_r values well below the 30% threshold, the seamless integration of Dy^{3+} ions into the Ca_3WO_6 lattice was confirmed, with no significant structural distortions. These results underscore the structural robustness and crystallographic suitability of Dy^{3+}-doped Ca_3WO_6 phosphors, establishing a strong foundation for their application in advanced luminescent applications.

The following eqn (1) is used to calculate the D_r:

$$D_r = \frac{R_s(CN) - R_d(CN)}{R_s(CN)} \times 100\% \quad (1)$$

where, R_s denotes the ionic radii of the substituted ions, and R_d indicates the ionic radii of the doping ions. The term CN refers to the coordination number. In the first case of Ca_3WO_6:Dy^{3+}, due to the closely matched ionic radii of Dy^{3+} (0.912 Å, CN = 6) and Ca^{2+} (1.00 Å, CN = 6),[14] Dy^{3+} ions probably substitute for Ca^{2+} sites within the host lattice. Subsequently, the calculated D_r for Dy^{3+} doping at Ca^{2+} site was computed to be 8.8 Å (<30%), strongly suggesting that Dy^{3+} ions are indeed replacing Ca^{2+} sites in the host matrix.[13]

3.2. Morphological observations

The surface morphology of phosphor materials significantly governs their luminescent efficiency and optical performance. To investigate the morphological attributes of the Ca_3WO_6:1.5 mol% Dy^{3+} phosphor, selected for its exceptional photoluminescence (PL) intensity, scanning electron microscopy (SEM) was performed using a Carl Zeiss Supra 55 instrument. Micrographs were acquired at resolutions of 200 nm, 1 μm, and 2 μm, providing a detailed depiction of the material's surface topography.

As shown in Fig. 3(a–d), the phosphor exhibits a heterogeneous microstructure, characterized by micro- and nano-sized grains with irregular shapes and a pronounced porous surface. This porosity likely results from the evolution of gaseous by-products during high-temperature calcination, contributing to the observed surface irregularities. Quantitative analysis of the SEM images reveals an average grain size ranging from a few nanometers to approximately 1 μm, reflecting the intricate morphological profile formed during the solid-state synthesis process.

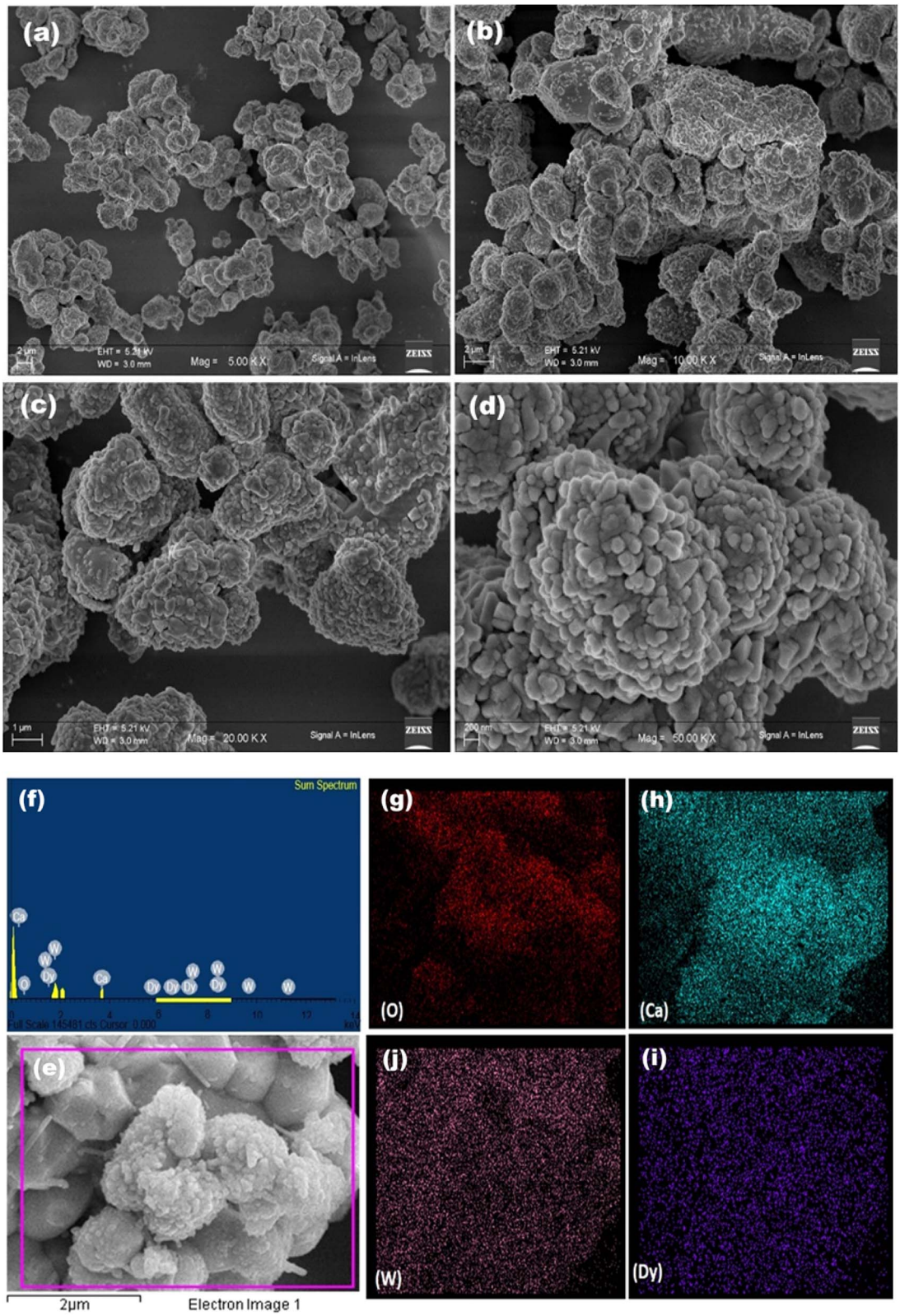

Fig. 3 (a–d) SEM micrographs of Ca_3WO_6:1.5 mol% Dy^{3+} phosphor at magnifications of 5k×, 10k×, 20k× and 50k×, respectively. (e) Selected area SEM micrograph, (f) EDAX spectrum and (g–j) elemental mapping of Ca_3WO_6:1.5 mol% Dy^{3+} phosphor for O, Ca, Dy and W, respectively.

To substantiate the morphological findings and confirm the elemental composition, energy-dispersive X-ray spectroscopy (EDAX) was conducted. The EDAX spectrum, illustrated in Fig. 3(e–j), verifies the presence of calcium (Ca), tungsten (W), oxygen (O), and dysprosium (Dy), aligning with the stoichiometric composition of Ca_3WO_6:1.5 mol% Dy^{3+}. Elemental

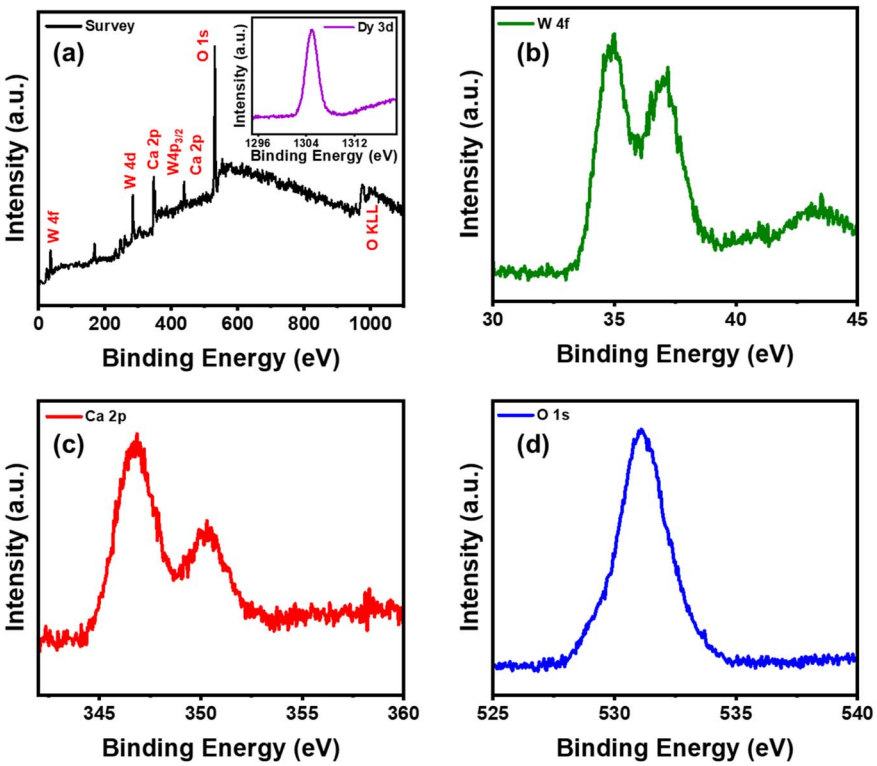

Fig. 4 (a) XPS survey spectra of Ca_3WO_6:1.5 mol% Dy^{3+} phosphor, inset shows the core-level spectra of Dy, (b–d) shows the core-level spectra of W, Ca and O, respectively.

mapped images further demonstrate the uniform distribution of these constituents across the phosphor matrix, affirming the homogeneous incorporation of Dy^{3+} ions despite their low doping concentration. This uniform dispersion is pivotal for ensuring consistent luminescence performance. Together, the SEM and EDAX analyses validate the structural, compositional, and morphological integrity of the Ca_3WO_6:1.5 mol% Dy^{3+} phosphor, highlighting its suitability for advanced photonic applications.

3.3. X-ray photoelectron spectroscopy analysis

To elucidate the surface chemical composition and oxidation states of the Ca_3WO_6:1.5 mol% Dy^{3+} phosphor, X-ray photoelectron spectroscopy (XPS) was conducted using an OMICRON Multiprobe Surface Analysis System under ultrahigh vacuum (base pressure: 5×10^{-11} torr). The XPS survey scan, presented in Fig. 4(a), confirms the presence of Ca, W, Dy, O, and trace carbon (C), consistent with the phosphor's stoichiometric formulation and surface characteristics.

Core-level XPS spectra of the W 4f region shown in Fig. 4(b) reveal two distinct spin–orbit split peaks, corresponding to W $4f_{7/2}$ and W $4f_{5/2}$, centered at binding energies of 35.2 eV and 37.2 eV, respectively. These peak positions, sensitive to the chemical environment of tungsten atoms, indicate that tungsten predominantly exists in the +6 oxidation state (W^{6+}, ~90%), with a minor contribution from the +5 oxidation state (W^{5+}, ~10%). This distribution underscores the stability of the WO_6^{2-} tungstate group within the Ca_3WO_6 lattice, with the minor W^{5+} component likely arising from localized surface defects or partial reduction during synthesis.

The Ca 2p core-level spectra shown in Fig. 4(c) exhibit two well-resolved peaks at 346.8 eV (Ca $2p_{3/2}$) and 350.4 eV (Ca $2p_{1/2}$), confirming the presence of Ca^{2+} ions in the phosphor matrix. For dysprosium, the Dy 4d peak, observed at a binding energy of 167 eV, aligns with the characteristic signature of Dy_2O_3, verifying that Dy^{3+} ions are successfully incorporated into the

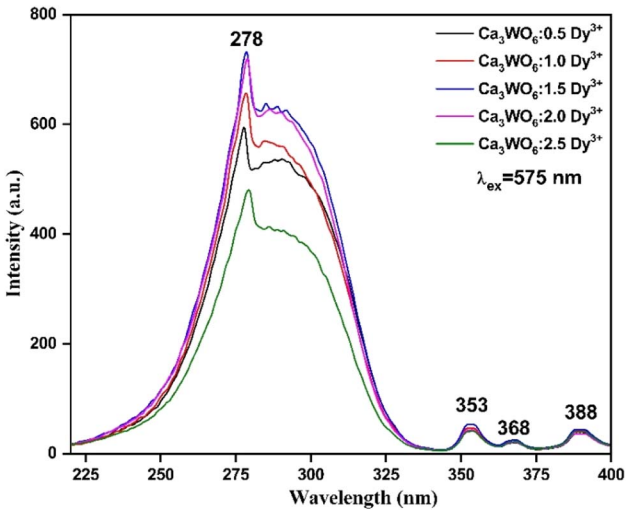

Fig. 5 PL excitation spectra of Ca_3WO_6:xDy^{3+} (x = 0.5–2.5 mol%) phosphors.

lattice. The low intensity of the Dy peak reflects the relatively low doping concentration (1.5 mol%), yet its clear detection affirms the uniform dispersion of the dopant as shown in inset of Fig. 4(a).

The O 1s core-level spectrum shown in Fig. 4(d) displays a broad peak centered at 531.2 eV, accompanied by shoulder features, indicative of multiple oxygen bonding environments. Deconvolution of the O 1s spectrum reveals four distinct contributions at 529.0 eV, 530.4 eV, 531.8 eV, and 533.2 eV, corresponding to lattice O^{2-}, W–O bonds, surface hydroxyl groups (OH^-), and adsorbed oxygen species, respectively. The dominance of the W–O peak highlights the structural integrity of the tungstate groups, while the presence of OH^- and adsorbed oxygen suggests minor surface interactions with the ambient environment.

This comprehensive XPS analysis not only validates the elemental composition and chemical states of the Ca_3WO_6:1.5 mol% Dy^{3+} phosphor but also provides critical insights into its surface chemistry. The findings confirm the successful integration of Dy^{3+} ions and the stability of the host lattice, reinforcing the phosphor's potential for high-performance luminescent applications in advanced photonic devices.

3.4. Photoluminescence analysis

To thoroughly investigate the luminescent properties of Dy^{3+}-activated Ca_3WO_6 phosphors, a comprehensive photoluminescence (PL) study was conducted across Dy^{3+} doping concentrations of 0.5–2.5 mol%.

Photoluminescence excitation (PLE) spectra, recorded at room temperature with an emission wavelength of 576 nm, are depicted in Fig. 5. These spectra reveal a complex array of optical transitions within the 220–500 nm range, characterized by broad charge transfer bands and sharp Dy^{3+} intra-4f transitions. Two prominent charge transfer bands dominate the 220–350 nm region, centered at 278 nm and ~300 nm. The 278 nm peak arises from electron transfer between the O^{2-} 2p and Dy^{3+} 4f orbitals, while the ~300 nm band is attributed to ligand-to-metal charge transfer involving O^{2-} and W^{6+} ions within the

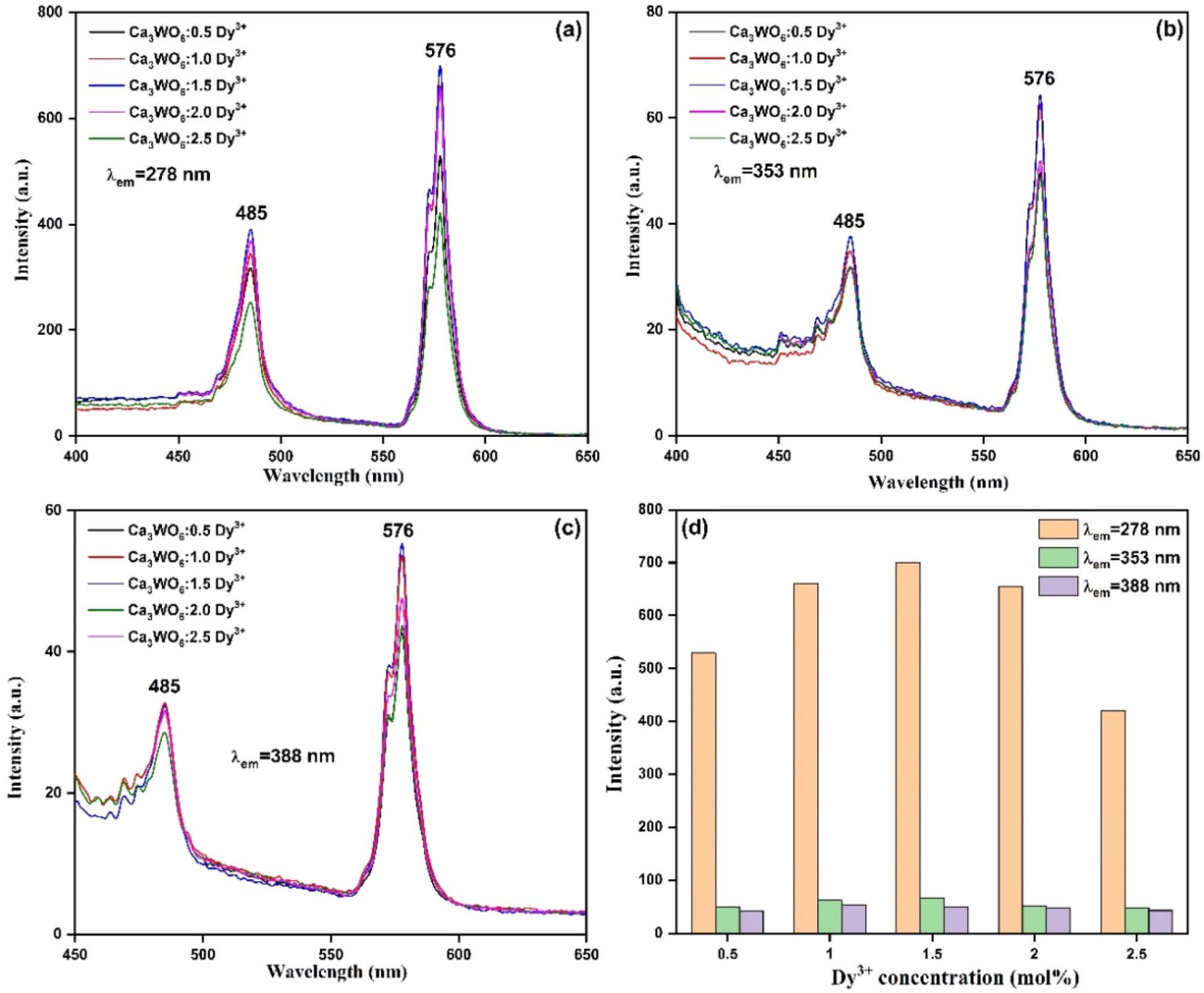

Fig. 6 PL emission spectra of Ca_3WO_6:xDy^{3+} (x = 0.5–2.5 mol%) phosphors recorded at (a) 278 nm, (b) 353 nm, and (c) 388 nm; and (d) plot of PL intensity as a function of Dy^{3+} concentration.

Ca_3WO_6 host lattice.[15] Additionally, distinct excitation peaks at 353 nm, 368 nm, and 388 nm correspond to Dy^{3+} transitions from the $^6H_{15/2}$ ground state to the $^6P_{7/2}$, $^6P_{5/2}$, and $^4I_{13/2}$ excited states, respectively, highlighting the versatility of Dy^{3+} as a dopant.[16,17]

Emission spectra of the Ca_3WO_6:D^{3+} phosphors, excited at 278 nm, 353 nm, and 388 nm, are presented in Fig. 6(a–c).[18,19] Regardless of excitation wavelength, the emission profiles consistently feature two intense peaks at 485 nm and 576 nm, corresponding to the characteristic Dy^{3+} transitions of $^4F_{9/2} \rightarrow {}^6H_{13/2}$ (blue) and $^4F_{9/2} \rightarrow {}^6H_{13/2}$ (yellow), respectively.[20–22] These radiative transitions, critical for white light emission, underscore the phosphors' potential in display and lighting applications. An energy level diagram of Dy^{3+} ions, shown in Fig. 7, elucidates the luminescence mechanisms, emphasizing the $^4F_{9/2}$ level as the primary emissive state driving efficient visible emissions through radiative and non-radiative pathways.[23,24]

The effect of Dy^{3+} doping concentration on luminescence intensity was systematically explored, as illustrated in Fig. 5 and 6(a–c). Emission intensity increases with Dy^{3+} content, peaking at an optimal concentration of 1.5 mol%, before declining due to concentration quenching, as shown in Fig. 6(d). This quenching, pronounced at 2.0 mol% Dy^{3+}, results from non-radiative energy transfer among closely spaced Dy^{3+} ions, facilitated by multipolar interactions or exchange mechanisms, which dissipate excitation energy and reduce luminescence efficiency.[25] These findings highlight the critical need for precise dopant optimization to maximize the luminescent performance of Ca_3WO_6:Dy^{3+} phosphors. To identify the exact mechanism of intensity quenching, the concept of critical distance is utilized, for which the following eqn (2) was used:[26,27]

$$R_c = 2\left(\frac{3V}{4\pi X_c N}\right)^{\frac{1}{3}} \quad (2)$$

where, V denotes the unit cell volume, N stands for the number of host cations in the unit cell, and X_c is the threshold doping concentration. As a result, the calculated value of R_c was determined to be 25.37 Å (>5 Å), strongly suggesting that multipolar interactions are responsible for the concentration quenching.[28,29]

The interplay between the Ca_3WO_6 host and Dy^{3+} ions significantly influences the phosphors' luminescent properties. The host lattice provides an optimal crystal field environment, enabling efficient energy transfer from the WO_6^{2-} tungstate groups to Dy^{3+} ions, which subsequently emit characteristic blue and yellow luminescence. The local symmetry and crystal field strength around Dy^{3+} ions, modulated by the host, further shape the emission spectra, color purity, and overall optical performance, reinforcing the phosphor's suitability for advanced photonic applications.

QY measurements reveal variations in luminescent efficiency with excitation wavelength. At 278 nm, the QY reaches 12%, indicating moderate efficiency, while at 353 nm and 388 nm, it decreases to 0.49% and 1.18%, respectively, reflecting lower efficiency at these wavelengths. In comparison, the commercial CREE phosphor achieves a QY of 37%, outperforming Ca_3WO_6:Dy^{3+}. These results underscore areas for further optimization to enhance the phosphors' efficiency, positioning Ca_3WO_6:Dy^{3+} as a promising candidate for next-generation display and lighting technologies.

3.5. PL decay analysis

To unravel the relaxation dynamics and energy transfer mechanisms underpinning the luminescent behavior of Dy^{3+}-doped Ca_3WO_6 phosphors, photoluminescence (PL) decay lifetime measurements were meticulously performed across samples with Dy^{3+} concentrations of 0.5–2.5 mol%. Decay kinetics offer profound insights into the temporal evolution of excited states, elucidating the balance between radiative and non-radiative processes within the phosphor system. Decay curves were acquired at room temperature under 278 nm excitation, with emission monitored at 576 nm, corresponding to the $^4F_{9/2} \rightarrow {}^6H_{13/2}$ transition of Dy^{3+} ions. These curves, depicted in Fig. 8

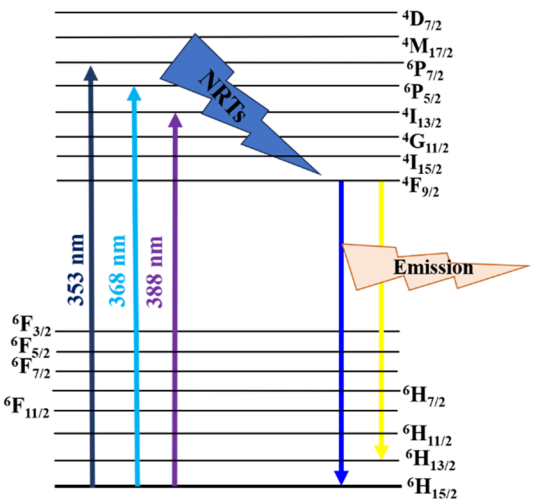

Fig. 7 Energy level diagram of Dy^{3+} ion and PL mechanism.

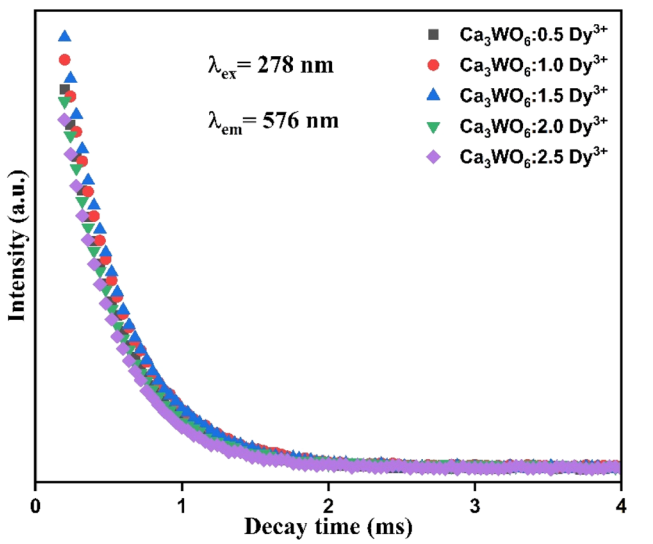

Fig. 8 PL decay curves of Ca_3WO_6:xDy^{3+} (x = 0.5–2.5 mol%) phosphors recorded with λ_{ex} = 278 nm and λ_{em} = 576 nm.

for Ca_3WO_6:xDy^{3+} (x = 0.5–2.5 mol%), were analyzed using sophisticated fitting techniques to derive precise lifetime parameters, capturing the intricate luminescence dynamics influenced by Dy^{3+} ion interactions within the Ca_3WO_6 host lattice.[30,31]

The decay profiles were best described by a bi-exponential decay model, indicative of heterogeneous relaxation pathways, and fitted using the following equation:[32]

$$I(t) = A_1 e^{(-t/\tau_1)} + A_2 e^{(-t/\tau_2)} \quad (3)$$

where, $I(t)$ represents the time-dependent PL emission intensity, A_1 and A_2 are the constants, and, τ_1 and τ_2 denote the short and long decay time constants, respectively. The presence of two distinct lifetime components suggests that Dy^{3+} ions occupy two unique crystallographic environments within the Ca_3WO_6 lattice. Ions embedded in deeper energy levels exhibit a faster decay (τ_1), while those in shallower levels display a slower decay (τ_2), reflecting variations in local coordination and electronic interactions. To quantify the overall luminescence lifetime, the average decay time for the $^4F_{9/2}$ level of Dy^{3+} was calculated using the weighted formula:[33]

$$\tau = \frac{A_1\tau_1^2 + A_2\tau_2^2}{A_1\tau_1 + A_2\tau_2} \quad (4)$$

The computed average lifetimes for the Ca_3WO_6:Dy^{3+} phosphors were calculated as 0.409 ms (0.5 mol%), 0.403 ms (1.0 mol%), 0.394 ms (1.5 mol%), 0.391 ms (2.0 mol%), and 0.373 ms (2.5 mol%). A discernible trend emerges: the lifetime progressively shortens with increasing Dy^{3+} concentration. This reduction is primarily driven by enhanced non-radiative energy transfer among neighboring Dy^{3+} ions, facilitated by their reduced inter-ionic distances at higher doping levels.[32] Such interactions, likely mediated by multipolar or exchange mechanisms, accelerate the depopulation of the $^4F_{9/2}$ excited state, resulting in shorter lifetimes. These findings illuminate the complex decay kinetics of the Ca_3WO_6:Dy^{3+} system, highlighting the pivotal role of dopant concentration in optimizing luminescent efficiency for advanced photonic applications, such as solid-state lighting and high-resolution displays.[30]

3.6. Temperature-dependent photoluminescence studies

To evaluate the thermal stability and color emission sensitivity of Ca_3WO_6:Dy^{3+} phosphors for solid-state lighting and high-power energy applications, temperature-dependent PL (TDPL) studies were conducted over a temperature range of 25–200 °C. The results, presented in Fig. 9(a), reveal that the emission peak intensity at 576 nm ($^4F_{9/2} \rightarrow {}^6H_{13/2}$) decreases steadily with rising temperature, while the peak position remains largely unchanged. Quantitative analysis indicates that the integrated emission intensity at 200 °C retains 59% of its room-temperature value, underscoring the phosphor's robust thermal stability. This intensity reduction is attributed to the diversion of excitation energy from the luminescent core toward non-radiative thermal emission pathways *via* lattice relaxation. These non-radiative transitions, associated with a Stokes shift, diminish PL emission due to thermal quenching effects.[34]

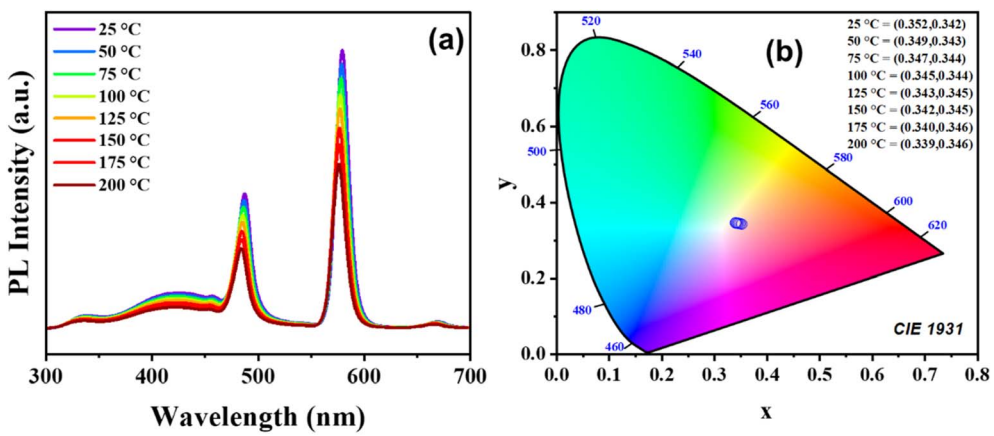

Fig. 9 (a) Temperature dependent PL emission spectra and (b) CIE chromaticity diagram of Ca_3WO_6:Dy^{3+} phosphor.

Table 2 Comparison of external quantum yield values of some reported phosphors to that of Dy^{3+}-doped Ca_3WO_6 double perovskite phosphor

S. no.	Host lattice	Dopant	External quantum yield	CIE coordinates	Reference
1	$Na_3Ba_2LaNb_{10}O_{30}$	Dy	45.35%	(0.362, 0.389)	35
2	La_2ZnTiO_6	Sm^{3+}, Dy^{3+}	52%	(0.497, 0.449)	36
3	$Sr_{0.98}Ga_2B_2O_7$	0.01Bi^{3+}, 0.01Dy^{3+}	65.4%	—	37
4	$KBaScSi_3O_9$	Dy	39%	(0.384, 0.418)	38
5	Ca_3WO_6	Dy^{3+}	59%	(0.352, 0.342)	Current work

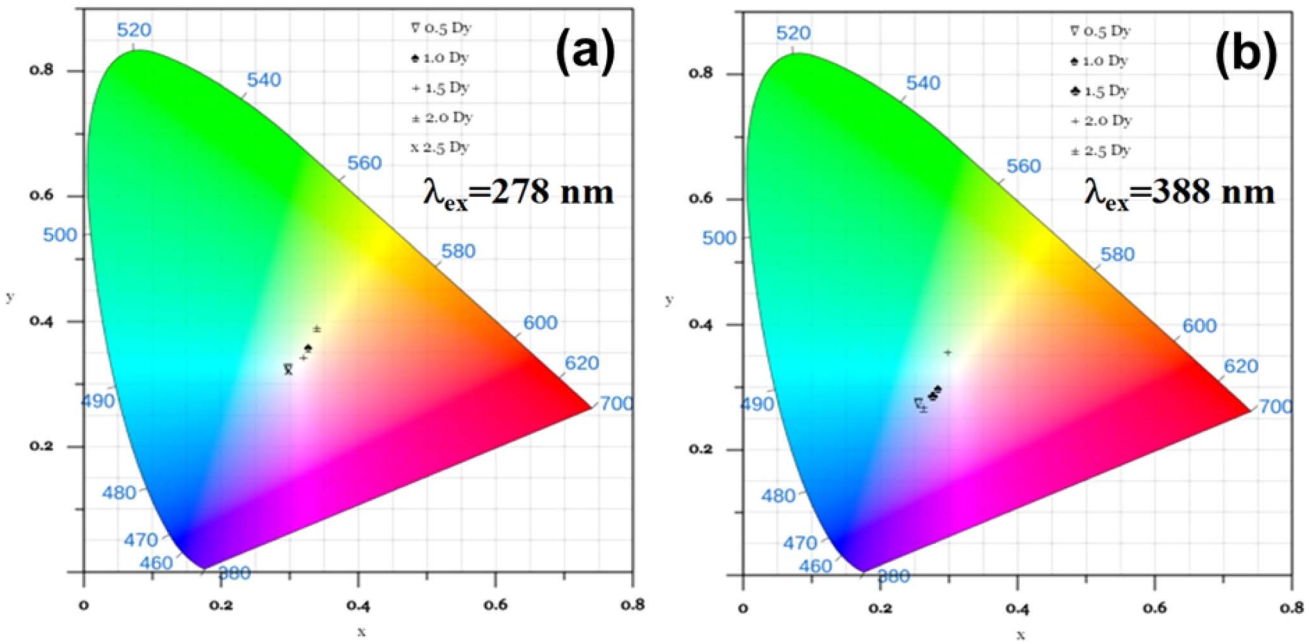

Fig. 10 CIE color coordinates of Ca_3WO_6:xDy^{3+} (x = 0.5–2.5 mol%) phosphors estimated for (a) λ_{ex} = 278 nm and (b) λ_{ex} = 388 nm.

The CIE chromaticity coordinates, plotted in Fig. 9(b), exhibit a temperature-dependent shift, with the phosphor's emission approaching the ideal white light coordinates (0.33, 0.33) as temperature increases. This trend suggests that elevated temperatures enhance the chromaticity alignment with optimal white light, offering potential for tailoring the phosphor's color properties in specific applications, such as white LEDs and displays. Comparative data from the literature, summarized in Table 2, further contextualize the thermal performance of Ca_3WO_6:Dy^{3+}, affirming its competitive standing among similar phosphor systems. These TDPL results highlight the phosphor's thermal resilience and tunable optical properties, positioning it as a promising candidate for high-performance luminescent applications under varying thermal conditions.

3.7. Photometric analysis

To assess the chromatic performance and applicability of Dy^{3+}-doped Ca_3WO_6 phosphors in advanced lighting and display technologies, a meticulous photometric analysis was conducted by determining their Commission Internationale de l'Éclairage (CIE) chromaticity coordinates. These coordinates provide a standardized framework for evaluating color quality, enabling precise quantification of the phosphors' emitted light within the visible spectrum.[38,39] Using photoluminescence (PL) emission data, CIE color coordinates were calculated for Ca_3WO_6:Dy^{3+} phosphors with Dy^{3+} concentrations of 0.5–2.5 mol%, under excitation wavelengths of 278 nm and 388 nm, to elucidate their chromatic behavior across varying conditions.

The results, vividly depicted in Fig. 10(a and b), showcase the CIE chromaticity coordinates for the phosphors under both excitation wavelengths. Under 278 nm excitation, the Ca_3WO_6:1.5 mol% Dy^{3+} phosphor yields coordinates of (0.319, 0.343), closely aligning with the ideal white light point of (0.333, 0.333) per CIE standards.[40,41] This near-ideal chromaticity highlights the phosphor's exceptional ability to produce high-quality white light, a critical attribute for next-generation display and lighting applications. Across all doping concentrations under 278 nm excitation, the CIE coordinates consistently fall within the white light region of the CIE diagram, affirming the robust white-emitting capability of the Ca_3WO_6:Dy^{3+} series. In contrast, under 388 nm excitation, the coordinates shift toward the bluish-white region, reflecting excitation-dependent variations in Dy^{3+} transition dynamics that subtly alter the emission type.[42]

The superior photometric performance under 278 nm excitation underscores the phosphors' potential as versatile candidates for optoelectronic applications. Their ability to deliver stable, tunable white light, as evidenced by their precise placement in the CIE chromaticity space, addresses the stringent requirements of modern display technologies. However, the QY of Ca_3WO_6:Dy^{3+} phosphors, particularly at longer excitation wavelengths (*e.g.*, 0.49% at 353 nm and 1.18% at 388 nm), is relatively low compared to the 12% QY at 278 nm and the 37% QY of commercial CREE phosphors. While the moderate QY at 278 nm supports niche applications, the lower QY at longer wavelengths may limit suitability for high-efficiency LED systems, necessitating further optimization to enhance luminescent efficiency. These findings position Ca_3WO_6:Dy^{3+} phosphors as promising materials with significant potential for tailored photonic applications, provided QY improvements are achieved.

4. Conclusions

This study comprehensively validates the synthesis, structural robustness, and superior luminescent properties of Dy^{3+}-doped

Ca_3WO_6 phosphors, optimized across 0.5–2.5 mol% Dy^{3+} concentrations, establishing their potential as high-efficiency materials for advanced white light-emitting displays. X-ray diffraction with Rietveld refinement confirmed a stable monoclinic $P2_1/c$ crystal structure, while SEM revealed a porous, agglomerated microstructure in the optimal 1.5 mol% Dy^{3+} phosphor, with particle sizes ranging from nanometers to micrometers, corroborated by EDAX's demonstration of uniform elemental distribution. XPS analysis verified Dy^{3+} incorporation, with the Dy 4d peak at 167 eV indicating Dy_2O_3 formation. Photoluminescence studies, monitored at 576 nm, displayed robust charge transfer bands at 278 nm and ~300 nm, alongside Dy^{3+} intra-4f transitions, with emission spectra under 278 nm, 353 nm, and 388 nm excitations showcasing intense blue (485 nm) and yellow (576 nm) emissions, peaking at 1.5 mol% Dy^{3+} before concentration quenching due to multipolar interactions. Decay kinetics showed lifetimes decreasing from 0.409 ms to 0.373 ms with rising Dy^{3+} content, reflecting enhanced non-radiative energy transfer. CIE chromaticity coordinates under 278 nm excitation (0.319, 0.343) closely approached the ideal white point (0.333, 0.333), affirming the phosphors' exceptional suitability for advanced white light-emitting display technologies.

Data availability

The data that support the findings of this study are available from the corresponding author upon reasonable request.

Author contributions

P. N. K. Chaitanya – data curation, investigation, writing original-draft, D. Haranath – formal analysis, methodology, writing – review & editing, D. Dinakar – formal analysis, writing – review & editing, M. Sree Ramana – supervision, formal analysis, K. V. R. Murthy – conceptualization, supervision, M. Rakshita – formal analysis, writing – review & editing, Govind Gupta – formal analysis, writing – review & editing.

Conflicts of interest

There are no conflicts of interest to declare.

Acknowledgements

The author, DH, expresses profound gratitude to the Department of Science and Technology (DST), Government of India, for their generous financial support through project #CRG/2021/007142, which was instrumental in advancing this research. MR is grateful to the Council of Scientific & Industrial Research (CSIR), Government of India, for providing financial support under various project *viz* CSIR – SRF #09/0922(11518)/2021-EMR-I.

References

1 J. Xue, Y. Guo, B. K. Moon, S. H. Park, J. H. Jeong, J. H. Kim and L. Wang, Improvement of photoluminescence properties of Eu 3+ doped SrNb 2 O 6 phosphor by charge compensation, *Opt. Mater.*, 2017, **66**, 220–229, DOI: 10.1016/j.optmat.2017.02.002.

2 T. Grzyb, A. Szczeszak, J. Rozowska, J. Legendziewicz and S. Lis, Tunable Luminescence of Sr $_2$ CeO $_4$:M $^{2+}$ (M = Ca, Mg, Ba, Zn) and Sr $_2$ CeO $_4$:Ln $^{3+}$ (Ln = Eu, Dy, Tm) Nanophosphors, *J. Phys. Chem. C.*, 2012, **116**, 3219–3226, DOI: 10.1021/jp208015z.

3 M. H. Im and Y. J. Kim, Energy transfer and multiple photoluminescence of LuNbO4 co-doped with Eu3+ and Tb3+, *Mater. Res. Bull.*, 2019, **112**, 399–405, DOI: 10.1016/j.materresbull.2019.01.009.

4 R. G. Kunghatkar, V. L. Barai and S. J. Dhoble, Synthesis route dependent characterizations of CaMgP2O7: Gd^{3+} phosphor, *Results Phys.*, 2019, **13**, 102295, DOI: 10.1016/j.rinp.2019.102295.

5 V. M. Krishna, S. Mahamuda, R. A. Talewar, K. Swapna, M. Venkateswarlu and A. S. Rao, Dy^{3+} ions doped oxy-fluoro boro tellurite glasses for the prospective optoelectronic device applications, *J. Alloys Compd.*, 2018, **762**, 814–826, DOI: 10.1016/j.jallcom.2018.05.191.

6 C. Wei, D. Xu, Z. Yang, Y. Jia, X. Li and J. Sun, Luminescence and energy transfer of Tm^{3+} and Dy^{3+} co-doped Na_3 $ScSi_2$ O_7 phosphors, *RSC Adv.*, 2019, **9**, 27817–27824, DOI: 10.1039/C9RA04727A.

7 Q. Sun, S. Wang, L. Sun, J. Liang, B. Devakumar and X. Huang, Achieving full-visible-spectrum LED lighting *via* employing an efficient Ce^{3+}-activated cyan phosphor, *Mater. Today Energy*, 2020, **17**, 100448, DOI: 10.1016/j.mtener.2020.100448.

8 C. Wei, D. Xu, J. Li, A. Geng, X. Li and J. Sun, Synthesis and luminescence properties of Eu^{3+}-doped a novel double perovskite Sr2YTaO6 phosphor, *J. Mater. Sci.: Mater. Electron.*, 2019, **30**, 2864–2871, DOI: 10.1007/s10854-018-0563-2.

9 K. Li and R. Van Deun, Obtaining Efficiently Tunable Red Emission in $Ca_{3-\delta}$ Ln $_\delta$ WO_6 :Mn^{4+} (Ln = La, Gd, Y, Lu, δ = 0.1) Phosphors Derived from Nearly Nonluminescent Ca_3 WO_6 :Mn^{4+} *via* Ionic Substitution Engineering for Solid-State Lighting, *ACS Sustain. Chem. Eng.*, 2020, **8**, 7256–7261, DOI: 10.1021/acssuschemeng.0c02444.

10 X. Zhao, J. Wang, L. Fan, Y. Ding, Z. Li, T. Yu and Z. Zou, Efficient red phosphor double-perovskite Ca3WO6 with A-site substitution of Eu^{3+}, *Dalton Trans.*, 2013, **42**, 13502, DOI: 10.1039/c3dt51029h.

11 T. H. Q. Vu, D. Stefańska and P. J. Dereń, Effect of A-Cation Radius on the Structure, Luminescence, and Temperature Sensing of Double Perovskites A_2MgWO_6 Doped with Dy^{3+} (A = Ca, Sr, Ba), *Inorg. Chem.*, 2023, **62**, 20020–20029, DOI: 10.1021/acs.inorgchem.3c02798.

12 N. Degda, N. Patel, V. Verma, K. V. R. Murthy and M. Srinivas, Luminescence and dosimetry approach in

terbium(III)-activated tungstate double perovskite, *Luminescence*, 2024, **39**, e4622, DOI: 10.1002/bio.4622.

13 G. Hu, S. Yi, Z. Fang, Z. Hu and W. Zhao, Luminescence properties of high thermal stability Sr2LaNbO6:xLn^{3+}(Ln^{3+}=Eu^{3+}/Sm^{3+}) phosphors with double-perovskite structures, *Opt. Mater.*, 2019, **98**, 109428, DOI: 10.1016/j.optmat.2019.109428.

14 R. D. Shannon, Revised effective ionic radii and systematic studies of interatomic distances in halides and chalcogenides, *Acta Crystallogr., Sect. A*, 1976, **32**, 751–767, DOI: 10.1107/S0567739476001551.

15 N. Prabhu, S. Agilan, N. Muthukumarasamy and T. S. Senthil, Enhanced photovoltaic performance of WO3 nanoparticles added dye sensitized solar cells, *J. Mater. Sci.: Mater. Electron.*, 2014, **25**, 5288–5295, DOI: 10.1007/s10854-014-2303-6.

16 Z. Yang, Y. Liu, C. Liu, F. Yang, Q. Yu, X. Li and F. Lu, Multiwavelength excited white-emitting Dy^{3+} doped $Sr_3Bi(PO_4)_3$ phosphor, *Ceram. Int.*, 2013, **39**, 7279–7283, DOI: 10.1016/j.ceramint.2013.02.044.

17 L. Fu, X. Yang, Z. Fu, Z. Wu and J. H. Jeong, Hydrothermal synthesis and tunable luminescence of CaSiO3:RE^{3+}(RE^{3+}=Eu^{3+}, Sm^{3+}, Tb^{3+}, Dy^{3+}) nanocrystals, *Mater. Res. Bull.*, 2015, **65**, 315–319, DOI: 10.1016/j.materresbull.2015.01.060.

18 T. Sh. Atabaev, H. H. T. Vu, H.-K. Kim and Y.-H. Hwang, Synthesis and optical properties of Dy^{3+}-doped Y2O3 nanoparticles, *J. Korean Phys. Soc.*, 2012, **60**, 244–248, DOI: 10.3938/jkps.60.244.

19 A. K. Vishwakarma, K. Jha, M. Jayasimhadri, B. Sivaiah, B. Gahtori and D. Haranath, Emerging cool white light emission from Dy^{3+} doped single phase alkaline earth niobate phosphors for indoor lighting applications, *Dalton Trans.*, 2015, **44**, 17166–17174, DOI: 10.1039/C5DT02436F.

20 P. Muralimanohar, G. Srilatha, K. Sathyamoorthy, P. Vinothkumar, M. Mohapatra and P. Murugasen, Preparation and luminescence properties of Dy^{3+} doped BaAlBO3F2 glass ceramic phosphor for solid state white LEDs, *Optik*, 2021, **225**, 165807, DOI: 10.1016/j.ijleo.2020.165807.

21 H. Wu, Z. Sun, S. Gan and L. Li, Luminescence properties of Dy^{3+} or/and Sm^{3+} doped $LiLa(WO4)_2$ phosphors and energy transfer from Dy^{3+} to Sm^{3+}, *Solid State Sci.*, 2018, **85**, 48–53, DOI: 10.1016/j.solidstatesciences.2018.09.013.

22 Y. Lian, Y. Wang, J. Li, Z. Zhu, Z. You, C. Tu, Y. Xu and W. Jie, Structural and optical properties of Dy^{3+}:YAlO3 phosphors for yellow light-emitting diode applications, *J. Rare Earths*, 2021, **39**, 889–896, DOI: 10.1016/j.jre.2020.06.012.

23 Q. Xu, J. Sun, D. Cui, Q. Di and J. Zeng, Synthesis and luminescence properties of novel $Sr_3Gd(PO4)_3$:Dy^{3+} phosphor, *J. Lumin.*, 2015, **158**, 301–305, DOI: 10.1016/j.jlumin.2014.10.034.

24 M. Gao, K. Li, Y. Yan, S. Xin, H. Dai, G. Zhu and C. Wang, Novel thermally robust warm white light emitting phosphor $Ca18Li_3Y(PO4)_{14}$:Dy^{3+}: Synthesis, crystal structure and luminescence property investigation, *J. Mol. Struct.*, 2021, **1228**, 129471, DOI: 10.1016/j.molstruc.2020.129471.

25 J. Zhao, D. Zhao, Z. Ma, M.-J. Ma, B.-Z. Liu, W.-J. Guo and G.-Y. Wang, Synthesis and photoluminescent properties of orange-emitting Sm^{3+}-activated $KPb4(PO4)_3$ phosphor for LEDs, *Displays*, 2019, **59**, 16–20, DOI: 10.1016/j.displa.2019.05.003.

26 N. Jain, B. P. Singh, R. K. Singh, J. Singh and R. A. Singh, Enhanced photoluminescence behaviour of Eu^{3+} activated ZnMoO 4 nanophosphors *via* Tb^{3+} co-doping for light emitting diode, *J. Lumin.*, 2017, **188**, 504–513, DOI: 10.1016/j.jlumin.2017.05.007.

27 N. P. Patel, N. Degda, V. Verma, K. V. R. Murthy and M. Srinivas, Thermally stable photoluminescence of Eu^{3+} doped strontium pyrophosphate: red emitting phosphor with high color purity, *New J. Chem.*, 2024, **48**, 5399–5411, DOI: 10.1039/D3NJ03994C.

28 Y. Zhou, Y. Li, H. Wu, X. Li and M. Gou, High temperature persistent luminescence in Tb^{3+} doped CaSr2Al2O6 phosphor, *Optik*, 2021, **242**, 167103, DOI: 10.1016/j.ijleo.2021.167103.

29 H. Ait ahsaine, M. Ezahri, A. Benlhachemi, B. Bakiz, S. Villain, J.-C. Valmalette, F. Guinneton, M. Arab and J.-R. Gavarri, Structural, vibrational study and UV photoluminescence properties of the system $Bi_{(2-x)}Lu_{(x)}WO_6(0.1 \leq x \leq 1)$, *RSC Adv.*, 2015, **5**, 96242–96252, DOI: 10.1039/C5RA19424E.

30 C. Kumari, R. Gopal, H. Yadav and J. Manam, SrNb2O6: Dy^{3+}: a single phase warm white light emitting phosphor for solid-state lighting, *J. Mater. Sci.: Mater. Electron.*, 2024, **35**, 638, DOI: 10.1007/s10854-024-12396-9.

31 R. Gopal, A. Kumar and J. Manam, Enhanced photoluminescence and abnormal temperature dependent photoluminescence property of SrWO4:Dy^{3+} phosphor by the incorporation of Li+ ion, *Mater. Chem. Phys.*, 2021, **272**, 124960, DOI: 10.1016/j.matchemphys.2021.124960.

32 J. Dalal, M. Dalal, S. Devi, A. Hooda, A. Khatkar, V. B. Taxak and S. P. Khatkar, Radiative and non-radiative characteristics of $Ca_9Bi(PO_4)7$:Eu^{3+} nano-phosphor for solid state lighting devices, *J. Lumin.*, 2019, **216**, 116697, DOI: 10.1016/j.jlumin.2019.116697.

33 S. Liu, J. He, Z. Wu, J. H. Jeong, B. Deng and R. Yu, Preparation and study on the spectral properties of garnet-type $Li_3Gd_3Te_2O_{12}$:Dy^{3+} single-phase full-color phosphor, *J. Lumin.*, 2018, **200**, 164–168, DOI: 10.1016/j.jlumin.2018.03.089.

34 M. Rakshita, A. A. Sharma, P. P. Pradhan, K. A. K. Durga Prasad, K. Jayanthi and D. Haranath, Highly efficient and self-activating $Zn_3V_2O_8$ phosphor for the fabrication of cool-white light emitting devices, *Ceram. Int.*, 2023, **49**, 16775–16785, DOI: 10.1016/j.ceramint.2023.02.038.

35 K. Poria, R. Lohan, S. Bhatia, A. Kumar, R. Singh, N. Deopa, R. Punia, J. S. Shahi and A. S. Rao, Lumino-structural properties of Dy^{3+} activated $Na_3Ba_2LaNb_{10}O_{30}$ phosphors with enhanced internal quantum yield for w-LEDs, *RSC Adv.*, 2023, **13**, 11557–11568, DOI: 10.1039/d3ra01260c.

36 C. Y. Chang, T. H. Hsu and C. L. Huang, Novel and thermostable double-perovskite La_2ZnTiO_6: Sm^{3+}, Dy^{3+} phosphors with high quantum efficiency, *Opt. Mater.*, 2023, **135**, 113361, DOI: **10.1016/J.OPTMAT.2022.113361**.

37 S. Yang, Y. Dai, Y. Shen, C. Duan, Q. Rao, H. Peng, F. Yang, Y. Shan and Q. Zhao, Blue emission from Sr0.98Ga2B2O7: $0.01Bi^{3+}$, $0.01Dy^{3+}$ phosphor with high quantum yield, *J. Alloys Compd.*, 2019, **810**, 151849, DOI: **10.1016/J.JALLCOM.2019.151849**.

38 K. Mariselvam and J. Liu, Judd-Ofelt analysis and visible luminescence of Sm^{3+}: MCZBP glass for reddish-orange laser and multi-colour display applications, *Solid State Sci.*, 2021, **115**, 106606, DOI: **10.1016/j.solidstatesciences.2021.106606**.

39 B. Fan, J. Liu, W. Zhou and L. Han, Luminescence properties of new red-emitting phosphor Li2Al2Si3O10:Eu^{3+} for near UV-based white LED, *Opt. Mater.*, 2019, **98**, 109499, DOI: **10.1016/j.optmat.2019.109499**.

40 B. C. Jamalaiah, M. Jo, J. Zehan, J. J. Shim, S. Il Kim, W.-Y. Chung and H. J. Seo, Luminescence, energy transfer and color perception studies of $Na_3Gd(PO_4)_2$:Dy^{3+}:Tm^{3+} phosphors, *Opt. Mater.*, 2014, **36**, 1688–1693, DOI: **10.1016/j.optmat.2014.01.016**.

41 D. Zhu, M. Liao, Z. Mu and F. Wu, Preparation and Luminescence Properties of $Ca_9NaZn(PO_4)_7$:Dy^{3+} Single-Phase White Light-Emitting Phosphor, *J. Electron. Mater.*, 2018, **47**, 4840–4844, DOI: **10.1007/s11664-018-6380-9**.

42 G. Zhang, L. Zhao, F. Fan, Y. Bai, B. Ouyang, W. Chen, Y. Li and L. Huang, Near UV-pumped yellow-emitting Ca_3TeO_6:Dy^{3+} phosphor for white light-emitting diodes, *Spectrochim. Acta, Part A*, 2019, **223**, 117343, DOI: **10.1016/j.saa.2019.117343**.